RASĀYAN *J. Chem.*
Vol. 16 | No. 4 |2239-2248| October - December | 2023
ISSN: 0974-1496 | e-ISSN: 0976-0083 | CODEN: RJCABP
http://www.rasayanjournal.com
http://www.rasayanjournal.co.in

KINETICS AND THERMODYNAMIC STUDIES OF PHOTO-CATALYTIC HYDROGEN GENERATION BY Au/Pt/TiO_2

Susmita A. Mandavgane✉, Sadhana Rayulu, Anushree A. Chilkalwar, Swapna M. Anjankar, Afsha Anjum Moinuddin, Tanvir Arfin and Akshat A. Mandavgane

Environmental Materials Division, CSIR-National Environmental Engineering Research Institute (CSIR-NEERI), Nehru Marg, Nagpur-440020, India

✉Corresponding Author: susmitamandavgane@gmail.com

ABSTRACT

Titania-supported Au-Pt nanoparticles have been prepared by the photo-deposition method employing platinum and gold particles on the titanium dioxide surface. The properties of the developed photocatalysts were characterized by two methods, such as UV-visible diffuse spectrophotometry (UV-Vis) and transmission electron microscopy (TEM). When loaded with gold and platinum particles, titanium dioxide's (TiO_2) photocatalytic activity significantly improved. This beneficial effect was attributed to an augmentation in the segregation of the electron-hole charge carriers generated by the photons. The kinetic and thermodynamic parameters were carried out, and they followed the Langmuir-Hinshelwood (L-H) mechanism. The amount of photo-induced hydrogen fabrication was studied, which depended on the sacrificial agent's concentration. It was found that the constant rate tends to increase as the concentration of ethanol increases. At 100 percent ethanol, there is a departure from the trend due to a change in the reaction mechanism. It was also observed that the rate increased with temperature. The different thermodynamic parameters like enthalpy of activation ($\Delta H^{\#}$), activation energy (E_a), entropy of activation ($\Delta S^{\#}$), and Gibb's free energy of activation ($\Delta G^{\#}$) were estimated for the reaction. Net energy recovery (NER) is a critical criterion for assessing the viability of conducting a photocatalytic process. Additionally, the current investigation revealed that the system containing 80% ethanol exhibited the greatest NER value.

Keywords: Gold-Platinum Doped Titania; Photo-Catalytic Hydrogen Generation; L-H Kinetics; Thermodynamic Parameters; Net Energy Recovery.

RASĀYAN *J. Chem.*, Vol. 16, No. 4, 2023

INTRODUCTION

Energy is the essential source required for a healthy life on earth. The most significant form of energy needed to balance the ecosystem is solar energy, but it cannot be adapted for application in terms of primary sources. Energy generated from fossil fuels helps in assisting and booming our everyday activities for sustaining life and incorporating industrial events. Researchers from parts of the country are effortlessly working hard to derive an alternative source of energy that is eco-friendly and readily acceptable to the environment. Hydrogen is considered the best option for the fuel needed in the future. Au, Ag, and Cu possess unique characteristics in terms of surface plasmon resonance (SPR). It is mainly the resonant oscillation of the free electron within the metals, as the frequency of the photon incident ties up with the frequency of the surface electron that oscillates in context with the restoring force of positively charged metallic nuclei.[2] Such metals can absorb light in the visible region, enabling them to be the essential component for solar irradiance, and therefore they have gained attraction for applications in photovoltaics and photodetectors.[3,4] Due to its substantial extinction coefficient, the Au particle is predominantly utilized in the configuration of a plasmonic metal.

In contrast, TiO_2 is classified as an electron-accepting n-type semiconductor on account of its attributes, including a substantial density of states (DOS) situated within the conduction band (CB).[5] Platinum plays a crucial role in impeding the recombination process of both electron (e-) and hole (h+) charges, hence functioning as a transient reservoir. The platinum surface facilitates the reaction of electrons with water or photon molecules, resulting in the formation of H* radicals. [6,7,8] It has been found that Pt nanoparticles do not show any visible light absorption, whereas they exhibit excellent catalytic activity. Hence, the utilization of bimetallic nanoparticles composed of gold (Au) and platinum (Pt) on titanium dioxide (TiO_2) holds

http://doi.org/10.31788/RJC.2023.1648617

significant potential for harnessing the advantages of surface plasmon resonance (SPR) for visible light absorption while simultaneously mitigating charge carrier recombination. Photocatalytic hydrogen production derived from water and the availability of sacrificial agents on semiconductors have gathered interest due to their advanced applications for the use of solar energy and also for the generation of eco-friendly hydrogen fuel.

The sacrificial agents present in the water are helpful in preventing the side reaction, or they can also suppress the photoinduced charges to recombine, leading to high efficiency. The application of alcohol in the form of scavengers has lots of potential owing to its high ability to generate hydrogen from both materials, such as water and alcohol.[9,10] In this study, making and figuring out how bimetallic Au/Pt/TiO_2 nanoparticles work as photocatalysts and how well they make hydrogen are the most important things. The Langmuir-Hinshelwood model is employed to elucidate the mechanisms underlying catalytic reactions. It is revealed that both types of reactions are absorbed first on the surface of the reaction.

In a similar study of kinetics, it is absolutely necessary to fit the experimental value to the general equation. Then only can it be confirmed that the reaction is regarding the mechanism. Kinetic and thermodynamic studies were also carried out for the photocatalytic reactions using Au, Pt, and TiO_2 to understand the mechanism of the reaction. To evaluate the feasibility of the photo-catalytic reaction, the net energy recovery (NER) is calculated for the different systems and then compared with each other.

EXPERIMENTAL

Materials

All chemicals, hexachloroplatinic (IV) acid (99.7%), tetra chloroauric (III) acid (99.7%), titanium oxide (99.9%), and ethanol (99.5%) from Merck Chemicals, were used as received. The TiO_2 powder (Degussa P25), along with anatase/rutile in the ratio of 86.3/13/7, was applied throughout the whole process without any change. Milli-Q water was employed to make the solution.

Preparation of Au/Pt/TiO_2 Catalysis

The synthesis of all photocatalysts was carried out using a photo deposition technique. A suspension was prepared in the inner radiation vessel by combining 150 mg of TiO_2 with 380 mL of deionized water. Ethanol was added as a sacrificial donor, along with metal precursors including 2.5% hexachloroplatinic (IV) acid and 1% tetrachloroauric (III). The suspension was generated using magnetic stirring. Photoreaction experiments were performed within the photocatalytic reaction system, which is made up of a borosilicate glass cylinder covered by aluminum foil and black tape on the outside part to ensure that it is highly exposed to UV light. The reaction mixture underwent illumination using a medium-pressure mercury lamp with a power output of 450 W for a duration of one hour. The solution was subsequently centrifuged at 6000 rpm, washed with distilled water to yield Pt and Au-deposited TiO_2 powder, and kept in a vacuum oven at a temperature of 80 °C for drying and evaporating the entire ethanol. It was made sure that, before the illumination process, the aqueous solution was cleared by the nitrogen gas to discard the excess oxygen molecules that would disturb the chemical reaction.

Hydrogen Evaluation

A borosilicate photochemical reactor with three necks was used to insert a fixed amount of bimetallic Au/Pt/TiO_2, distilled water, and ethanol. It had a glass jacket internally coated with an illumination chamber and a chiller connection to enable the mercury lamp to work. Here again, before the irradiation process, the solution was made clear by using nitrogen to ensure total oxygen removal. At regular intervals, the H_2 content in the sample was estimated automatically by the gas chromatograph (Shimadzu 2014), along with the 5A plot column and thermal conductivity detection.

Catalysis Characterization

UV-DRS spectra were analyzed using an Agilent UV-Vis/NIR spectrophotometer. Absorbance spectra of all materials were analyzed with the same instrument, which measures the dispersion of metal on the semiconductor. The samples were subjected to transmission electron microscopy analysis using a Phillips CM100 electron microscope with an operating voltage of 100 kV.

RESULTS AND DISCUSSION

TEM Studies

The synthesis of Au-Pt bimetals was achieved using the photodeposition method. Figure-1 illustrates the presence of interface interactions between platinum on the gold surface and platinum on titania. The dark contrast clarifies the occurrence of metal particles. In Fig.-1a, the TEM image exhibits that the material is morphologically spherical in nature, and no separate Au and Pt nanoparticles were seen. It also showed that Au and Pt are well distributed randomly on the TiO_2 crystal surface. The sizeable TiO_2 matrix was observed to be bright, whereas Au and Pt nanoparticles were generally small dark spots. Figure-1b illustrates that the mean diameter of an Au-Pt bimetallic nanoparticle falls within the range of 3 to 5 nm. It was also observed that Pt and Au had an interaction between them in comparison to the Pt-Au/TiO_2 catalyst. In a study conducted by Na et al., it was observed that Pt and Au species undergo aggregation and an increase in particle size to 5–6 nm for the Pt-Au-IM catalyst and 4-5 nm for the Pt-Au-DP catalyst following impregnation and deposition-precipitation processes. It was not an easy task to identify the definite formation of Pt nanoparticles from Pt-Au/TiO_2, clarifying that there is a miscibility of Pt with the Au particles. It is commonly believed that the miscible character and availability of Pt on the surface act as responsible features for high photocatalytic action. As a result, our approach guarantees the activation of the plasmonic behavior exhibited by gold nanoparticles and the excellent electrical conductivity characteristic of platinum. In the course of this procedure, it is imperative to acknowledge the necessity for electronic differentiation between the thin layer of Pt on Au nanoparticles and the Pt-Au alloy, as compared to the approach recommended for Pt + Au. By observation made regarding the high splitting of water or overall splitting, the assumption is given that Pt plays a critical role in separating electron-hole pairs, which is mainly because of the presence of a sensitizer and co-catalyst. SPR, because of visible light absorption using Au, has to be central to local electromagnetic field improvement, and the way the equal has an impact on the nearby Pt layers has not always been recognized to date. The nano-Pt islands or layers that are in contact with gold or situated between neighboring gold layers must be subjected to the local electromagnetic field due to the presence of Au-SPR.

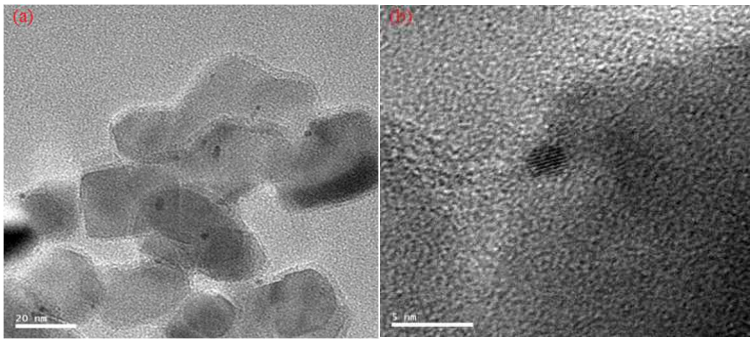

Fig.-1: TEM Images of Au-Pt/TiO_2 (a) High Range, (b) Low Range

UV-Visible Spectroscopy Studies

The UV-visible spectroscopy was tested for all four samples in Fig.-2. The Au-Pt interaction and optical properties were analyzed from the spectra. There is no significant difference between all frequencies up to 400 nm, but there is an appropriate sharp absorption threshold around 350 nm for TiO_2. When Pt was deposited on the surface of TiO_2, the color changed from white to gray, and a significant difference was noticed in the ranges of 400 to 600 nm. With the interaction of the Pt surface and TiO_2, the occurrence of an absorption band was observed. Chen et al. further asserted that Pt-TiO_2 exhibited an optical absorption mechanism inside the visible-light spectrum, rendering it a good candidate for harnessing energy from visible light.[12] Again, Au has deposited the color purple with the formation of the plasmonic peak at 550 nm. Various parameters, such as particle size, shape, and the dielectric constant of the medium, were responsible for the position and shape of the plasmonic peak.[13] For the interconnection of two metals, the absorption peaks were found to be influenced by the bimetallic structure. The deposition of both Au and Pt on TiO_2 changes the color to purple-dark grey, as observed in the spectra. Shah *et al.*[14] suggested the development of bimetallic dispersions, which is dependent on the two parameters, namely the

thermodynamics and kinetics, of the distinct components. The decrease in intensity and the selective blue shift are due to the predominating deposition of Pt on the Au surface, which also shows a modification in the catalyst's electronic interaction; these results are also supported by TEM micrographs.

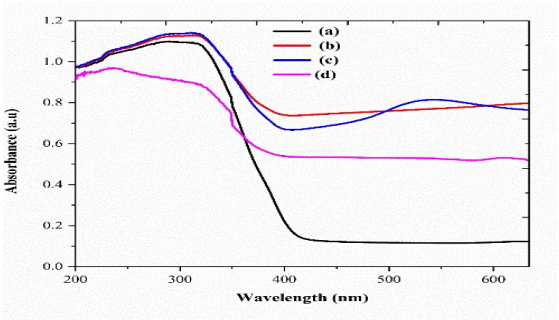

Fig.-2: UV Images of (a) TiO_2, (b) Pt-TiO_2, (c) Au-TiO_2, and (d) Au-Pt-TiO_2

Kinetic Studies

The Impact of Ethanol Concentration

The photocatalytic hydrogen generation kinetics using a sacrificial agent in the anatase phase of TiO_2 dispersions through UV irradiation are represented by the Langmuir-Hinshelwood model, as shown in Fig. 3.15–16. For each percentage of ethanol used during the process, the same trend is followed. As the concentration changes rapidly in terms of electron donors within the reaction, the rate of hydrogen generation increases as it reacts through the irreversible process with the photo-generated holes and oxygen, thereby increasing the speed of hydrogen formation. Figure-3 illustrates the impact of varying ethanol concentrations on the pace at which hydrogen is produced. The rate of hydrogen tends to increase in a non-linear form with an increase in initial ethanol concentration (C_0), and at high ethanol concentrations, it is leveled off. The saturation state reached a high ethanol concentration making it clear that there exists a severe conflict between the substrate and the reactant on the surface of Pt and Au nanoparticles. From the above, it can be concluded that the optimum state is determined in the area where the rate is high.[17] It was revealed that the Langmuir-Hinshelwood model could be applied to describe the dependence rate on the concentration. Supporting information: Figure-S1 shows the effect of a 100% ethanol concentration. Therefore, the rate changes in the term of C_o (ethanol) by a Langmuir-Hinshelwood model are represented as given below:

$$-r = \frac{dC(H_2)}{dt} = \frac{kKC}{1+KC} \qquad (1)$$

Where r, k, K, and C are designated as the rate of hydrogen production, the limiting rate constant of reaction at maximum under the given experimental condition (mg L^{-1} min^{-1}), the adsorption constant of ethanol (Lmg-1), and the concentration of hydrogen generated at any time t during degradation (mg L^{-1}) respectively. The Langmuir-Hinshelwood equation was directly determined by employing the relationship for the reaction rate, r, and $kKC/(1+KC)$ as in Eq.(1).

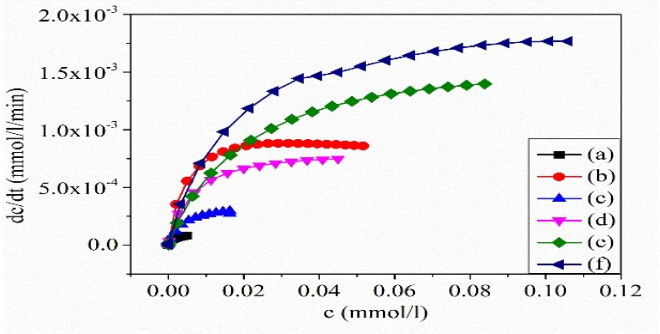

Fig.-3: Langmuir – Hinshelwood Plot of the rate of Hydrogen Production at Different Ethanol Concentration (a) 1%, (b) 5%, (c) 10%, (d) 25%, (e) 60%, and (f) 80%

Based on the linear transformation of Langmuir – Hinshelwood isotherm, which is as follows:

$$\frac{1}{r}=\frac{1}{kK}\times\frac{1}{C}+\frac{1}{K} \qquad (2)$$

Which envisages a straight line of 1/r versus 1/C in Fig.-4. The linear equation clarifies that the L-H model is well fitted for degradation kinetics, indicating saturation-type kinetics permitting the calculation of the values of k and K from the slope and intercept of a plot. The various parameters k and K are given in Table 1 for different ethanol concentrations.

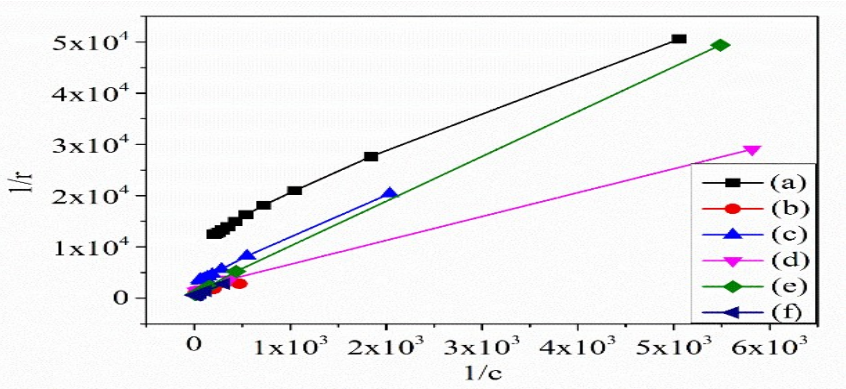

Fig.-4: Langmuir – Hinshelwood Plot of 1/r vs. 1/c at Different Ethanol Concentration (a) 1%, (b) 5%, (c) 10%, (d) 25%, (e) 60%, and (f) 80%

Table-1: Various Ethanol Concentrations with Rate Constant and Adsorption Coefficient

Percentage of ethanol	Rate constant (k) mol $L^{-1}min^{-1}$	Adsorption coefficient (K) $Lmol^{-1}$
1	8.66E-05	1466.09
5	2.05E-04	389.19
10	3.53E-04	287.68
25	8.53E-04	171.82
60	1.42E-03	79.21
80	2.03E-03	66.01
100	9.27E-05	356.20

The variation of the rate constant is studied by varying the concentration of ethanol, as shown in Fig.-5, and it was observed that the rate constant exhibits a linear relationship with the ethanol concentration due to higher rates of hole consumption, preventing the recombination of hole and electrons. It can be concluded from the above that it is a first-order reaction. The plot for the rate constant in the context of ethanol concentration is a straight line along the 2.35 E-5 slope.

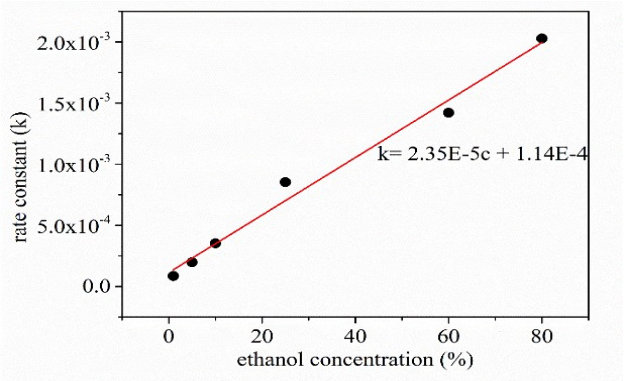

Fig.-5: Effect of Different Percentages of Ethanol Concentration on Rate Constant

The decrease in the adsorption coefficient for various ethanol concentrations is observed with a rise in the ethanol concentration, as depicted in Fig.-6. The presence of high ethanol concentrations on the surface of $Au/Pt/TiO_2$ nanoparticles clearly covers the majority of available sites, thereby decreasing the rate of electron transfer toward the surface. It was observed that at low ethanol concentrations, the adsorption

coefficient was at its maximum, and as soon as the ethanol concentration was increased, it led to a decline in the adsorption coefficient. The same trend is observed by Kumar *et al.*[18]

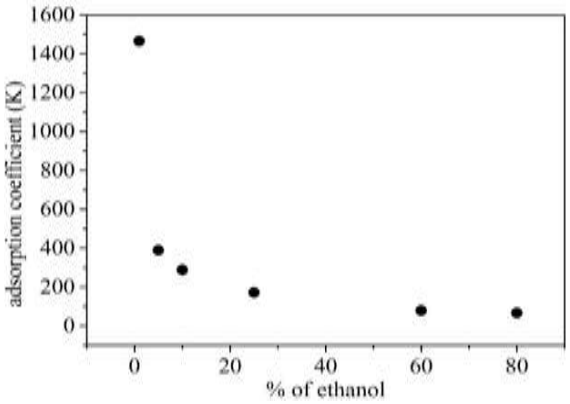

Fig.-6: Effect of Different Percentage of Ethanol on Adsorption Constant

Thermodynamic Studies

The thermodynamic parameters were calculated using different thermodynamic relations.[20] According to the Arrhenius equation, the rate of the reactions is influenced by the temperature, as given below:

$$k = Ae^{-E_a/RT} \quad (3)$$

Where T represents the absolute temperature, A represents the frequency factor, E_a signifies the activation energy, and R denotes the gas constant.

The equation can be further simplified by applying the natural log on both sides.

$$\ln k = \ln A - E_a/RT \quad (4)$$

As shown in Figure 7, the value of E_a was estimated using the Arrhenius plot (ln k vs 1/T), and its slope is $-E_a/R$. The value of $\Delta S^{\#}$ was also measured by the equation (5):

$$\ln A = \ln\left(k_B T/h\right) + \Delta S^{\#}/R \quad (5)$$

Where h denotes the Planck constant and k_B signifies the Boltzmann constant.

The value of ΔH was measured by the equation as shown below:

$$\Delta H^{\#} = E_a - RT \quad (6)$$

The value of ΔG was also estimated by the equation as shown below:[21]

$$\Delta G^{\#} = \Delta H^{\#} - T\Delta S^{\#} \quad (7)$$

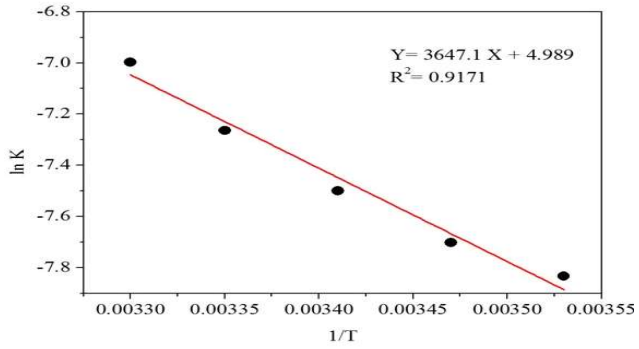

Fig.-7: Arrhenius Plot of Photocatalytic Hydrogen Generation

The literature previously mentioned has reported an E_a value ranging from 5 to 30 kJ/mol for the photocatalysis reaction.[22] In the present study, the activation energy was found to be 30.272 kJ/mol. All the different values of kinetic and thermodynamic terms, namely k, K, $\Delta S^{\#}$, $\Delta G^{\#}$, and $\Delta H^{\#}$ are calculated for the

system at different temperatures and are presented in Table-2. The rate constant's increase in response to temperature is evident and can be elucidated through the application of Maxwell's distribution of atomic energies and the Arrhenius equation. The steady adsorption decreases with temperature, which follows the fact that adsorption is always accompanied by the production of heat. Consequently, as per Le Chatelier's theory, a decrease in temperature results in a corresponding increase in the value of adsorption. The Arrhenius activation energy is the expression derived from the Arrhenius equation (Eq.-5) and is the parameter established by experimentation reflecting the sensitivity of reaction rate in correspondence to temperature. The activation energy for photocatalytic hydrogen generation in the temperature range of 283 to 303 K was found to be 30.272 kJ/mol, which is quite small and hence indicates that the photocatalytic reaction is affected by the temperature. It means that if the activation energy is low, the reaction rate is high.[23] The clarification of this fact was achieved by formulating the surface rate constant (k) in the L-H model. The respective action of the process can be cleared by photonic activation since irradiation is the main agent for electron-hole pair formation and is liable to initiate a photoreaction. The photocatalytic process can be performed without heat, but it can also be operated at room temperature. The value of real activation energy for the system is nil; however, the value of E_a is also small at a medium temperature ranging from 20°C to 80°C.The thermodynamic parameters of photocatalytic hydrogen generation are described. According to the data presented in Table-2, it can be observed that there is a positive correlation between temperature and the values of k. This implies that as the temperature increases, the rate of ethanol concentration also increases. The values of $\Delta H^{\#}$ were positive and demonstrated the endothermic characteristic of the process, whereas the values of $\Delta S^{\#}$ were negative for the process of photocatalysis. The negative $\Delta S^{\#}$ obtained states that the reactant in the ground state has a less ordered structure in comparison to the transition state.[24] The negative $\Delta S^{\#}$ is also credited with the association of ethanol adsorption on the $Au/Pt/TiO_2$ surface.[25] The value of $\Delta G^{\#}$ is also positive, reflecting that the reaction is non-spontaneous. This positive $\Delta G^{\#}$ is mainly due to the activated state, which forms a well-solvated structure and is governed by the negative entropy of the activation value. It also exhibits the barrier as free energy when it shifts towards the activated state from the reactant state.

Table-2: Kinetic and Thermodynamic Parameters of Photo-Catalytic Hydrogen Generation at Different Temperatures

S.No.	Temperature (K)	Rate Constant (k)	Adsorption Constant (K)	$\Delta H^{\#}$ ($kJmol^{-1}$)	$\Delta S^{\#}$ ($kJK^{-1}mol^{-1}$)	$\Delta G^{\#}$ ($kJmol^{-1}$)
1	283	4.161E-04	810.479	27.9192	-0.2031	85.3876
2	288	4.466E-04	732.211	27.8777	-0.2032	86.4033
3	293	5.226E-04	642.795	27.8361	-0.2034	87.4197
4	298	6.780E-04	469.200	27.7945	-0.2035	88.4369
5	303	9.825E-04	357.035	27.7530	-0.2036	89.4547

Energy Efficiency Analysis

Net energy efficiency was estimated from the ratio between the chemical energy of hydrogen and the overall energy input into the system in the form of energy needed for pumping, cooling, compression, and electricity, as shown in Fig.-8. The system consists of two parts, such as input and output. EI, E2, E3, E4, E5, and E6 are the energy inputs through ethanol, from the pump, from the agitator, from the chiller, through light, and energy outputs from generated hydrogen, respectively. It was presumed that the high heating value (HHV) of H_2 was 286 KJ/mol. The net energy efficiency is approximately 0.5%. The analysis yielded a quantitative methodology for assessing the energy production of the system in relation to the energy consumption necessary for its optimal operation. It also permits investors to recognize cost-effective methods and face the difficulties of a barrier to the growth of new innovative technologies.[26] The results make it clear that a net energy efficiency of 0.5% is presently reachable. The current ability can be significantly raised by enhancing the process, reducing the requirements for heat, creating more efficient subassemblies, and improving photo-catalytic reactor efficiency.

The assessment of water splitting for the generation of H_2 by applying TiO_2 photocatalyst within the distilled water had become a difficult task because of the quick combination of the photo-generated conduction band (CB) electron and valance bond (VB) holes. The addition of an electron donor, such as a

sacrificial reagent or hole scavengers, results in irreversible reactions with photo-generated valence band (VB) holes.

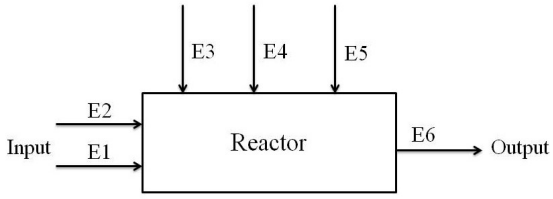

Fig.-8: Net Energy Recovery (NER) of the Photo-Catalytic System (Laboratory Scale)

This leads to an enhancement of the photocatalytic process of electron/hole separation, ultimately resulting in a high quantum efficiency. For sustaining the production of H_2, continuous addition of electron donors is needed as the donors are captured in the photocatalytic reaction. It has achieved the best-desired outcome for water splitting, as at 80% ethanol, the hybrid water splitting reaction was achieved. But at 100% ethanol, no water-splitting reaction has occurred, as shown in Fig.-9.

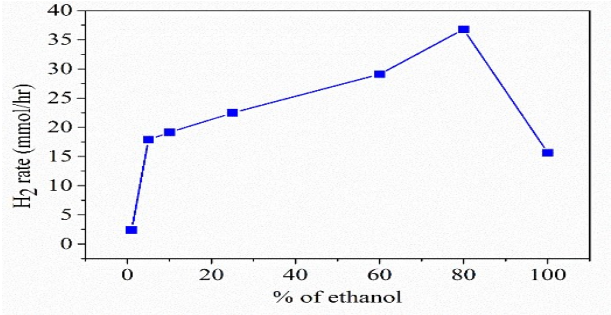

Fig.-9: Effect of Percentage of Ethanol on the Rate of Hydrogen Generation

The experimental results indicate that the reaction proceeded through the generation of surface ethoxide and hydroxyl species, which were produced via dissociative adsorption at the Pt, Au, and TiO_2 interfaces. In the vicinity of the interface, the H_2 atoms of the hydroxyl undergo effective degradation facilitated by the electrons originating from the metal particles. Conversely, the ethoxide acts as a hole trap, a phenomenon that may not be observable under conditions of 100% ethanol concentration. According to Fig.-10, there is a positive correlation between the percentage of ethanol and the rate of ethanol consumption. Finally, it can be concluded that net energy increased to 80% of the ethanol concentration, mainly because of the dissociative adsorption.

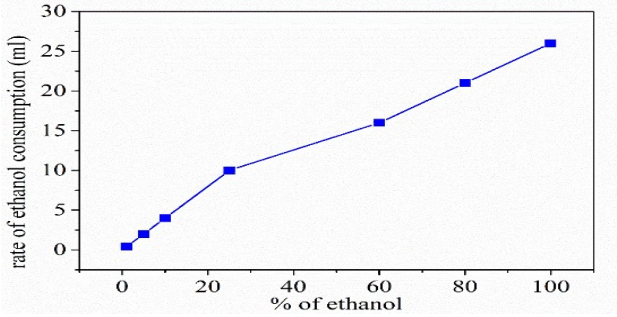

Fig.-10: Effect of Percentage of Ethanol on the Rate of Ethanol Consumption

The net energy recovery can be calculated as:

$$\text{Net Energy Recovery} = (\text{Output})/ (\text{Input})*100 \quad (8)$$

The calculated values are shown in Fig.-11. The data demonstrates a positive correlation between concentration and NER, with a linear increase detected up to 80%, after which a drop in the NER values was observed. Therefore, % of NER value depends on the concentration.

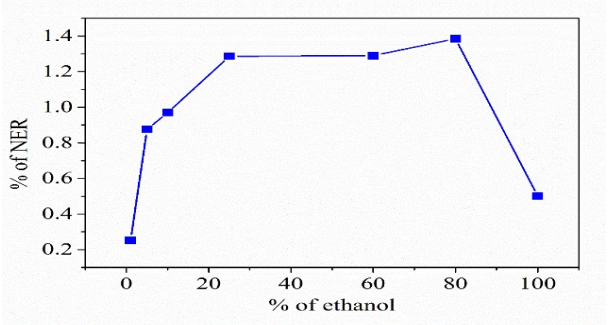

Fig.-11: Effect of Percentage of Ethanol on the Percentage of Net Energy Recovery

CONCLUSION

The kinetics associated with the process of photocatalytic hydrogen generation were successfully modeled through the utilization of an approximation of the Langmuir-Hinshelwood rate equation. The current investigation revealed a direct correlation between the concentration of the sacrificial agent, ethanol, and the rate constant of the reaction, indicating that an increase in ethanol concentration leads to a proportional rise in the rate constant. The adsorption coefficient decreases with an increase in the concentration of ethanol. Au/Pt/TiO_2 was expanded from the L-H model. With the help of experiments, the kinetic evaluation was performed to fit the data to the L-H model. It was successfully done, leading to the formation of relevant parameters as well. It was noticed that the photocatalytic hydrogen generation was not affected by temperature, as the value of E_a was found to be in the range of a few kJ mol^{-1}. The thermodynamic parameters of photocatalytic hydrogen generation are also explained. The value of $\Delta H^{\#}$ obtained is positive, indicating that the reaction is endothermic, and the value of $\Delta G^{\#}$ is also positive, which indicates non-spontaneous behavior. The positive value of $\Delta G^{\#}$ is observed since the activated state is in the form of a well-solvated structure lying within the reaction intermediates, and the ethanol molecules are assisted by the negative $\Delta S^{\#}$, which also suggests that the complex formation is greater in comparison to that of the reactant. It was found that the system with 80% ethanol has the highest NER value. The activation parameters for the surface rate constant (k) are represented as needed in metal nanoparticle systems. It confirms the credibility of the L-H model for investigating the behavior of nanoparticles and their kinetics during ethanol concentration. Such obtained details can be used in the catalysis of nanoparticles dealing with the surface reaction. On the other hand, it can be further utilized for surface behavior studies of nanoparticle incorporation by different stabilization systems. Additionally, it can aid in acquiring knowledge concerning the catalytic characteristics of metal nanoparticles and developing a more comprehensive comprehension of the reaction mechanism from a surface science perspective.

ACKNOWLEDGEMENTS

This work has been completed by financial support received under the TAPSUN Project (NWP-56).

CONFLICT OF INTERESTS

The authors declare that there is no conflict of interest.

AUTHOR CONTRIBUTIONS

All the authors contributed significantly to this manuscript, participated in reviewing/editing and approved the final draft for publication. The research profile of the authors can be verified from their ORCID ids, given below:

Sadhana Rayalu https://orcid.org/0000-0002-9517-4139
Susmita Mandavgane https://orcid.org/0000-0002-5982-1810
Anushree A. Chilkalwar https://orcid.org/0000-0002-2565-0064
Swapna M. Anjankar https://orcid.org/0009-0002-5099-3648
Afsha Anjum Moinuddin https://orcid.org/0009-0008-0279-3792
Tanvir Arfin https://orcid.org/0000-0002-5051-614X
Akshat Mandavgane https://orcid.org/0009-0001-0660-8645

REFERENCES

1. M. L. Brongersma, N. J. Halas and P. Nordlander, *Nature Nanotechnology,* **10(1)**, 25(2015), https://doi.org/10.1038/nnano.2014.311
2. J.Y. Park, L. R. Baker and G. A. Somorjai, *Chemical Review,***115(8)**, 2781(2015), https://doi.org/10.1021/acsphotonics.7b00695
3. S. Mubeen, J. Lee, W. Lee, N. Singh, G. D. Stucky, and M. Moskovits, *ACS Nano,* **8(6),** 6066(2014), https://doi.org/10.1021/acsomega.7b00394
4. M.W. Knight, H. Sobhani, P. Nordlander and N. J. Halas, *Science,* **332(6030)**, 702(2011), https://doi.org/10.1126/science.1203056
5. A. Furube, L. Du, K. Hara, R. Katoh, M. Tachiya, *Journal of American Chemical Society,* **129(48)**, 14852(2007), https://doi.org/10.1021/ja076134v
6. T.A. Egerton, J. A. Mattinson, *Journal of Photochemistry and Photobiology A: Chemistry* **194(2)**, 283(2008), https://doi.org/10.1155/2016/4231467
7. S. A. Mandavgane; *Materials Today: Proceedings,* **29,** 213(2020), https://doi.org/10.1016/j.matpr.2020.05.478
8. S. A. Mandavgane, N. P. Mohabansi and M. K. N. Yenkie, *Emerging Material Research*, **3(3)**, 144(2014).
9. N. L. Wu, M. S. Lee, Z. J. Pon and J. Z. Hsu, *Journal of Photochemistry and Photobiology A*, **163(1)**, 277(2004), http://dx.doi.org/10.4236/ojpc.2011.12005
10. S. A. Mandavgane and M. K. N. Yenkie, *Rasayan Journal of Chemistry*, **4(3)**, 640(2011).
11. H. Na, T. Zhu, Z. Liu, *Catalytic Science & Technology,* **4(7)**, 2051(2015).
12. H.W. Chen, Y. Ku, Y. L. Kuo, *Water Research*, **41(10)**, 2069(2007).
13. E. Ozbay, *Science*, **311**, 189(2006), https://doi.org/10.1126/science.1114849
14. A. Shah, Latif-ur-Rahman, R. Qureshi, Zia-ur-Rehman. *Reviews on Advanced Materials Science*, **30**, 133(2012).
15. M. A. Barakat, R.I. Al-Hutailah, M. H. Hashim, E. Qayyum, J. N. Kuhn, *Environmental Science and Pollution Research*, **20(6)**, 3751(2013), https://doi.org/10.1007/s11356-012-1306-1
16. P. M. Słomkiewicz, P.M. *Applied Catalysis A,* **269**, 33(2004).
17. P. Ncube, N. Bingwa, H. Baloyi, R. Meijboom, *Applied Catalysis A,* **495**, 63(2015), https://doi.org/10.1016/j.apcata.2015.01.033
18. K. V. Kumar, K. Porkodi, A. Selvaganapathi, *Dyes and Pigments,* **75(1)**, 246(2007), http://dx.doi.org/10.1016/j.dyepig.2006.05.035
19. J. Kim, C. A. Henao, T. A. Johnson, D. E. Dedrick, J. E. Miller, E. B. Stechel, C. T. Maravelias, *Energy Environmental Science,* **4(9)**, 3122(2011)
20. J. Panwar, L. Joshi, R. Ameta and D. Soni, *Rasayan Journal of Chemistry*, **16(3)**, 1326(2023), http://doi.org/10.31788/RJC.2023.1638260
21. T. Arfin, Rafiuddin. *Desalination*, **284**, 100(2012), http://dx.doi.org/10.1016/j.desal.2011.08.042
22. F. Zhang, J. Zhao, T. Shen, H. Hidaka, E. Pelizzetti, N. Serpone, *Applied Catalysis B,* **15**, 147(1998), https://doi.org/10.1016/S0926-3373(97)00043-X
23. J. E. Brady, G. E. Humiston, *General Chemistry*, John Wiley & Sons, New York, (1986).
24. A. Petek, M. Krajnc, *International Journal of Chemical Kinetics*, **44(10)**, 692(2012)**,** https://doi.org/10.1002/kin.20712
25. C. S. Consorti, F. R. Flores, J. Dupont, *Journal of the American Chemical Society*, **127(34)**, 12054(2005), https://doi.org/10.1021/ja051834q
26. X. Zhan, Q. Wang, F. Wang, Y. Wang, Z. Wang, J. Cao, M. Safdar, J. He, *ACS Applied Materials & Interfaces*, **6**, 2878(2014), http://dx.doi.org/10.1002/9783527696109.ch26

[RJC-8617/2023]